Original Research Article

Membrane fouling on the surface of nZVI@PVDF membrane and infrared spectroscopy-multivariable curve resolution analysis of membrane fouling

ABSTRACT

Few studies focused on the constraints of membrane fouling on nanomaterial-decorated modified membranes. Xanthan gum (XG) and humic acid (HA) belonging to dissolved organic matter are the main substances in membrane fouling, and their interaction affects the membrane fouling process. In this study, the fouling process of nZVI@PVDF membranes used to filter different concentrations of XG and HA were investigated by infrared spectroscopy-multivariable curve resolution analysis. The results showed that the decay of membrane flux was proportional to the content of TEP. When XG content was 25 %, membrane fouling was the most serious. XG played a major role in the pollution process of the nZVI@PVDF membrane, and the interaction between HA and XG had an impact on the formation process of TEP in water samples. When the content of XG was 60 %, the membrane fouling was the lightest, which was related to the humic acid size and the structure of the nZVI@PVDF membrane. It was found by SEM that the main contribution to fouling was the formation of XG on the membrane surface pollution layer. Experiments showed that the mixed solution of HA and XG will aggravate the fouling of the nZVI@PVDF membrane, but there may be an optimal ratio that can greatly reduce the fouling of the membrane.

Comment [en1]: The abstract does not include the results of the IR-ATR and MCR-ALS analyses on the membrane, and it does not clearly convey the study's findings. The abstract should comprehensively represent the content of the entire article. Additionally, the language and word choice in the article should be refined for better clarity and readability.

Keywords: Membrane fouling, nZVI@PVDF membrane, Xanthan gum, Humic acid

1. INTRODUCTION

Facing the severe problems of water shortage and water pollution, membrane separation technology plays an important role in industrial wastewater purification and seawater desalination [1-3]. According to the pore size, the membrane can be divided into microfiltration membrane, ultrafiltration membrane (UF), nanofiltration membrane, and reverse osmosis membrane [4]. UF membrane technology has higher efficiency and lower energy costs because UF membrane's pore size ranges from 10 A to 1000 A and requires low-pressure filtration at 0.1 - 0.5 MPa. [5]. Ultrafiltration(UF) membra remove bacteria and most viruses, which prevent water-related diseases and microbial death and improve effluent [6]. Wide-used polyvinylidene fluoride (PVDF) has excellent film-forming properties, stability, chemical stability, stability, and mechanical strength, making it a suitable material for preparing porous separation membranes.

Comment [en2]: Pay attention to the punctuation errors, and the citations are not properly linked to the reference list.

Recently, nanoscale zero-valent iron (nZVI) has been widely used in groundwater and industrial wastewater treatment due to its extremely small particle size, high specific surface area, and strong iron reducing power, showing excellent treatment effect [7]. However, nZVI particles have a strong aggregation trend, which is due to the strong magnetic attraction between particles [8].Therefore, nZVI particles for water treatment will reduce the reactivity due to the reduced surface area. The combination of functional nanomaterials with PVDF membranes provides an excellent opportunity to degrade pollutants, improve osmotic flux, and change hydrophilicity [9]. Pd/Fe nanoparticles (NPs) were immobilized in hydrophilically polyacrylic acid (PAA)/PVDF membrane to decrease the aggregation of Pd/Fe nanoparticles [10]. Nano

UNDER PEER REVIEW

Pd/Fe-based PVDF membrane had been successfully used in treating trichloroacetic acid [10], trichloroethylene [11], polychlorinated biphenyls [12], etc. In Our previous study, nZVI-modified PVDF membranes (nZVI@PVDF membranes) were functional successfully prepared by a simple and easy-to-follow filter-press coating method and was applied in the ultrafiltration process to treat 2-chlorophenol (2-CP) wastewater [13]. Due to the hydrophobicity of the PVDF membrane, serious membrane fouling is more likely to occur, which shortens the service life of the membrane, resulting in higher costs [14]. Simple surface coating with nZVI can improve both hydrophilicity and have little effect on the internal structure of the membrane. However, this method is often easy to plug the membrane pores, resulting in the decrease of the average pore size and porosity of the separation membrane, which makes it difficult for water molecules to penetrate the separation membrane and the water flux decreases sharply [15]. However, there is little literature on the fouling performance of the nanomaterial-modified ultrafiltration membrane.

Membrane contamination is due to the accumulation of organic matter, inorganic matter, or organisms on the membrane surface and inside the membrane pores [16]. Among these dissolved organic matters (DOMs) in wastewater have been considered as a key factor in membrane fouling [17]. In general, humic substances, proteins, and polysaccharides that belong to DOMs have been identified as the principal foulants that could block the membrane pores, and reduce permeate flux [18].Different properties of DOMs make them more difficult to solve the membrane fouling problem. Humic substances are the main component of DOMs and are considered to be one of the most serious membrane contaminants. Xanthan gum (XG), with unique rheological properties and good water solubility, is an extracellular polysaccharide of microorganisms with extensive functions [19]. XG molecules in a water environment are easy to combine with dissolved organic matter in water to form copolymers. The membrane contamination caused by the mixing of different organic pollutants is more complex due to its synergistic effect [20]. For example, the interaction between polysaccharides and proteins, such as humic acid (HA), may also increase membrane fouling during membrane filtration.In the process of studying the formation mechanism of membrane fouling, the mechanism of membrane fouling caused by the interaction among HA and XG is rarely reported. Notably, the release of iron ions will be accompanied by the use of nZVI@PVDF modified membranes, and the effect of the interaction between iron ions and organic matter on membrane contamination is worth studying.

Transparent exopolymer particles (TEP) is a gel-like acidic polysaccharide widely distributed in the ocean and wastewater, whose role in membrane fouling has attracted wide attention [21]. TEP is closely related to membrane fouling for the following reasons. Firstly, TEP has a high viscosity, which makes TEP easy to attach to the membrane surface and form a hydrogel layer, resulting in large membrane resistance [22]. Secondly, TEP has a three-dimensional structure and a large specific surface area, which is colonized by microorganisms [21]. Finally, the deformable TEP can under pressure go through pores smaller than its particle size by bending, breaking, and dispersing [23].To analyze the components of pollutants and explore the interaction between pollutants.IR-ATR (infrared attenuated total reflection) technology is adopted, which can reflect the structural information of pollutant functional groups in the process of membrane fouling, and its characterization of pore space distribution on the membrane surface is effective [24].The main drawback of this method is that the spectrum on each pixel is overlap different pollution components, so it is difficult to distinguish different components [25].Multivariable curve resolution-alternating least-squares analysis (MCR-ALS) assumes that the spectrum of each pixel in the image is a linear combination of a series of pure spectral signals. The pixel spectrum is preprocessed and decomposed into pure components of its contribution [26].The analysis method considered the complete spectral profile to identify compounds and visualize their distribution in the samples, to classify different chemical regions [27].MCR-ALS was used to characterize the characteristics of membrane fouling, and the results were rapid and easy to explain and evaluate membrane fouling from chemical and biological perspectives.

In this study, the analytical methods of IR-ATR and MCR-ALS were combined to build an infrared imaging platform for membrane fouling. The fouling of nZVI@PVDF modified membrane by HA, SA, and XG during ultrafiltration was studied for the first time. The identification of pollutants, the evaluation of membrane pore blockage, and the visualization of membrane surface pollution were carried out.The mechanism of membrane fouling caused by the interaction between HA and XG during the formation of membrane fouling was studied. Understanding TEP-induced modified membrane fouling mechanisms during ultrafiltration is of primary importance for developing effective fouling control and prevention strategies, and for improving membrane filtration performance..

Comment [en3]: What the mean?

2. MATERIAL AND METHODS

2.1 Preparation of nZVI@PVDF modified membrane

The nZVI preparation method used in this study was the liquid phase transformation method [13].A certain amount of dried nZVI was weighed, transferred to anhydrous and anaerobic ethanol, and then put into a bottle. Ultrasonic was carried out in an ultrasonic cleaner to make nZVI dispersed evenly.Then the anhydrous ethanol containing nZVI was poured into the ultrafiltration cup, and the nZVI was uniformly coated on the PVDF membrane (Zhongke Ruiyang

UNDER PEER REVIEW

Membrane Technology Co., Beijing, China) surface by nitrogen pressure.The membrane was washed three times with anaerobic ultrapure water aeration for 30 min in advance, and finally, the nZVI@PVDF modified ultrafiltration membrane coated with nZVI was obtained.The coating amount of nZVI used in this study was 2 mg/cm2, and the filtration area of the membrane was 36.32 cm2.

2.2 nZVI@PVDF modified membrane for ultrafiltration treatment of simulated wastewater

The total concentration of pollutants in the mixed solution was 100 mg / L, and the proportions of XG were 0 %, 25 %, 50 %, 60 %, 75 % and 100 %, respectively.The ultrafiltration experiment was performed using a cup filter for dead-end filtration, and the specific experimental device was shown in Fig.1. Firstly, the nZVI@PVDF modified membrane was fixed in the cup filter, and then the simulated water sample was poured into the cup filter. The magnetic stirrer was used to continuously and slowly stir water samples.The upper end of the cup filter was connected with a nitrogen bottle, and the pressure was adjusted to 0.1 MPa when filtering. The mass of the filtrate was recorded at a time interval of 10 s through the data acquisition software provided by the electronic balance. The PVDF ultrafiltration membrane was used in the experiment and immersed in ultrapure water for 24 h before use.

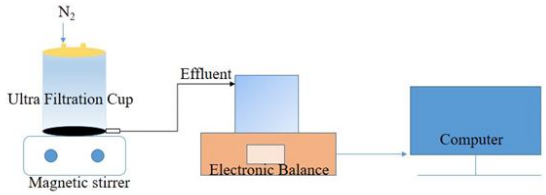

Fig.1. Diagram of ultrafiltration experimental setup.

2.3 TEP characterization

Alcian blue 8GX (0.02 %) was dissolved in 0.06 % acetic acid to prepare Alcian blue solution. The solution was filtered with a 0.05 μm pore water filter membrane to remove the influence of substances in Alcian blue on TEP test results. A total of 50 mL mixed solution of membrane pollution source was passed through 0.22 μm aperture of water system filter membrane under 0.2 bar pressure (keeping low pressure during filtration to protect TEP from destruction) and then dyed with 1 mL alcian blue solution for 5 s. The filter was washed with 1 mL ultrapure water.The filter membrane after dyeing was taken out and immersed in 5 mL of 80 % sulfuric acid for 2 h. During the immersion, the sample tube was shaken 3 – 5 times to ensure that alcian blue was completely dissolved in sulfuric acid.Finally, the absorbance of alcian blue in sulfuric acid solution was measured with a spectrophotometer at the wavelength of 612 nm using a 1 cm colorimetric dish. The average value of each sample was obtained after three repeated measurements.The concentration of TEP was finally expressed by the equivalent of xanthan gum per liter of water, namely mgXeq / L.

2.4 Characterization of membrane fouling

2.4.1 Membrane flux

The calculation formula of membrane flux (J) is:

$$J=V/T\times A \quad (2.1)$$

In the formula, J is the membrane flux (m / s), T is the sampling time (s), V is the volume of filtrate in the sampling time (m^3), A is the membrane filtration area (m^2).The degree of membrane fouling in this study is characterized by the attenuation of specific flux (J/J_0), where J represents the membrane flux at any time in the filtration process, and J_0 represents the initial membrane flux in the filtration process.With J/J_0 as the ordinate axis and the filtration time as the abscissa axis, the change of specific flux in the filtration process was plotted to reflect the change of membrane fouling.

2.4.2 Infrared imaging platform for surface contamination of modified membrane

Comment [en4]: In the abstract, it is mentioned that the simulated wastewater consists of HA, SA, and XG. Explain in more detail about these three components in the preparation of simulated wastewater.

Comment [en5]: Must 300 dpi

UNDER PEER REVIEW

The nZVI@PVDF membrane after filtration of simulated wastewater was dried at room temperature. The membrane surface was divided into 136 points(5 mm × 5 mm), and then the IR-ATR measurement (Nicolet iS10, Germany) was performed on each point.Test conditions: scan times: 32; resolution: 4; the wavenumber ranged from 4000 cm^{-1}~550 cm^{-1}.The infrared data obtained from the test were aggregated into the spectral matrix and imported into Matlab R2018b software for analysis by using the MCR-ALS script program. After several iterations of the ALS algorithm, the data of 136 points can be decomposed into the infrared spectrum and concentration distribution of pollutants on the membrane surface.Finally, the infrared image of the polluted film was obtained by drawing with software Origin 2019b.

2.4.3 SEM characterization

A scanning electron microscope (FE-SEM-EDS, Quant 250 FEG, FEI Corporation). was used to observe and characterize the surface morphology of the film. The test conditions were as follows: 220 V (± 10%), 50 Hz.Working temperature: 15 ~ 20 °C.Working humidity: < 80%.

3. RESULTS AND DISCUSSION

3.1 Effects of different mixing ratios of HA and XG on flux attenuation

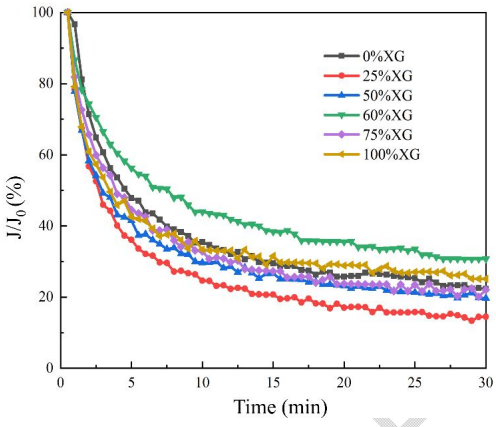

Fig. 2. Membrane flux attenuation of nZVI/PVDF modified membrane for filtering simulated water samples with different xanthan gum content

In this study, the effect of the composition of HA and XG in simulated water samples (total concentration of 100 mg/L) on membrane pollution was explored by changing the content of XG (0%, 25%, 50%, 60%, 75%, 100%) within 1h filtration cycle. Fig. 2 showed the relationship between membrane-specific flux and filtration time of nZVI@PVDF modified membrane in the process of filtering simulated water samples under 0.1 MPa. When the simulated water sample contained XG, the membrane flux of the simulated water sample decreased rapidly in the first 5 min of filtration and then decreased slowly after the first 5 min.When the filtration time reached 30 min, the membrane flux remained basically unchanged.When the content of XG was 60%, the specific flux of the membrane decreased the least. This means that the membrane fouling was the lightest, and the specific flux after 30 min was 30.7%.When the content of XG was 25%, the specific flux of the membrane decreased most. The membrane fouling was the most serious obviously, and the specific flux after 30 min was only 14.5%. Compared with pure HA and pure XG water samples, the membrane flux ofXG and HA mixed water samples was lower than that of single component water samples except for 60% XG content.This means that the membrane fouling was more serious, and the degree of membrane fouling decreased first and then increased with the content of XG.

Table 1 TEP content under different XG content

Comment [en6]: Must 300 dpi

Comment [en7]: Provide a deeper explanation and references as to why the 25% concentration has low flux, why 60% concentration has lower fouling, and what phenomena occur at 100%.

Comment [en8]: The discussion is still unclear. In the figure, there is no review related to HA, yet in the discussion, it is mentioned without an explanation about HA and XG. The sentence "Compared with pure HA and pure XG water samples, the membrane flux of XG and HA mixed water" has not been explained properly.

UNDER PEER REVIEW

content ofXG	Absorbance	TEP（mgXeq/L）
25	0.165	84.65
50	0.078	38.17
60	0.121	31.91
75	0.067	61.05

In order to determine the interaction between organic matter and polysaccharides, the correlation between TEP of HA and XG mixed solution and membrane fouling was worth studying.The TEP values for different XG contents are shown in Table 1.The measured value of TEP decreased first and then increased with the increase of XG content in the mixed solution.When the content of XG in the mixed solution is 25%, the TEP measurement value is the highest, reaching 84.65 mg Xeq/L.When the XG content was 60%, the measured value of TEP was the lowest, only 31.91 mg Xeq/L.This result corresponds to the attenuation of membrane flux in Fig. 2, indicating that membrane pollution was positively correlated with TEP in water samples.Therefore, the TEP value can reflect membrane fouling to some extent.

3.2 Different HA and XG mixing ratios correspond to changes in the IR-ATR spectrum

Fig.3 showed the infrared spectra of HA and XG pure components. It can be seen from Fig.3(a) that HA had a broad absorption peak at 3350 cm-1, representing O-H stretching vibration; the peak at 2970 cm^{-1}~2850 cm^{-1} was related to aliphatic C-H stretching vibration; The peak at 1724 cm^{-1} was caused by the stretching vibration of the C=O bond of the carbonyl group; the absorption peak at 1605 cm-1 was the aromatic C=C, COO-; the absorption at 1244 cm^{-1} was the C-O stretching of the carboxyl group Caused by vibration; 1027 cm-1 was related to carbohydrate CO stretching vibration. It can be seen from Fig. 3(b) that XG had a broad absorption peak at 3275 cm^{-1}, which represented the -OH group; 1602 cm-1 and 1398 cm^{-1} belonged to the COO- group.

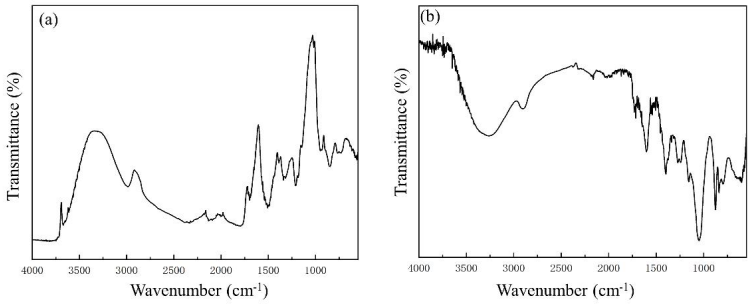

Fig.3 Infrared spectra of HA (a) and XG (b)

The MCR-ALS method was used to decompose the original data measured by IR-ATR into component spectra and their concentration data. Four components can be obtained, namely XG, HA, PVDF, and nZVI. The correlation coefficient R2 obtained by iteration of each infrared spectrum data matrix can reach more than 99.99%, and the relevant characteristic peaks in the infrared spectrum of each component obtained can also correspond to the infrared spectrum of the pure component, indicating the MCR-ALS analysis The results obtained are very reliable.

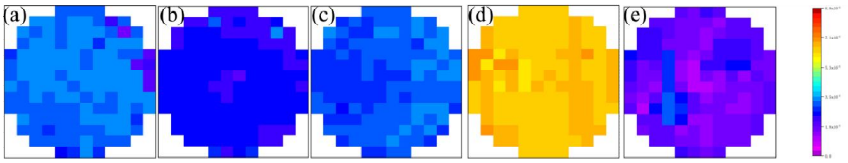

Fig.4 The surface of the membrane is contaminated by HA after filtering the simulated water sample for 1 hour under different mixing ratios of HA and XG.(XG content: a-0%, b-25%, c-50%, d-60%, e-75%)

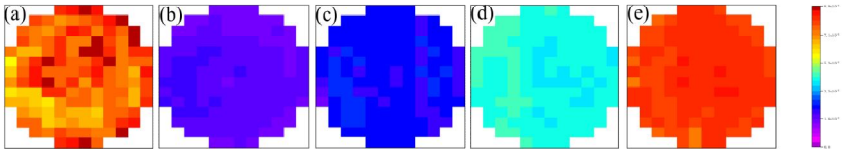

Fig. 5 The surface of the membrane is contaminated by XG after filtering the simulated water sample for 1 hour under different mixing ratios of HA and XG.(XG content: a-25%, b-50%, c-60%, d-75%, e-100%)

The concentration data obtained from the analysis are mapped to 136 points on the membrane surface one by one. The HA and XG pollution distribution diagrams on the membrane surface after filtering the simulated water sample for 1 h under different mixing ratios are shown in Fig. 4 and Fig. 5. When filtering pure HA and XG solutions of the same concentration, as shown in Fig. 4 (a) and Fig. 5 (e), the residue of XG on the membrane surface was significantly greater than that of HA. EPS, composed of polysaccharides, proteins, and humic substances, had been considered to cause serious membrane fouling. While polysaccharides usually have the most serious effect on the decrease of membrane flux [28]. Therefore, SA had a higher pollution potential than HA. When the XG content was 25% and 75%, the main residual contaminant on the film surface was XG, which was consistent with the large TEP value in Table 1. When the XG content was 60%, the main contaminant on the membrane surface was HA, which was consistent with the result of the smallest TEP measurement. When the XG content was 50%, the main contaminants on the membrane surface were HA and XG. The results also showed that TEP has a certain connection with membrane fouling.

Comment [en9]: In the discussion section, I have not found the correlation of the simulated wastewater used in the study, as it only mentions the concentration of XG and does not include HA. Therefore, it is unclear how the distribution of HA can be accounted for. It would be better to explain whether XG can convert into HA or to add details about how this process occurs.

3.3 The dynamic change of the film surface pollution corresponds to the IR-ATR spectrum

To investigate the dynamic changes of the membrane surface pollution during the filtration process, two special XG contents (25%, 60%) were selected during the membrane flux attenuation process. The membrane surface with different filtration times was characterized by infrared, combined with MCR-ALS analysis of the changes of the components on the surface of the membrane. Since the membrane flux tends to be flat or even basically unchanged after the filtration time reaches 20 min, the filtration time selected for the study of dynamic changes is 5 min, 10 min, and 20 min.

UNDER PEER REVIEW

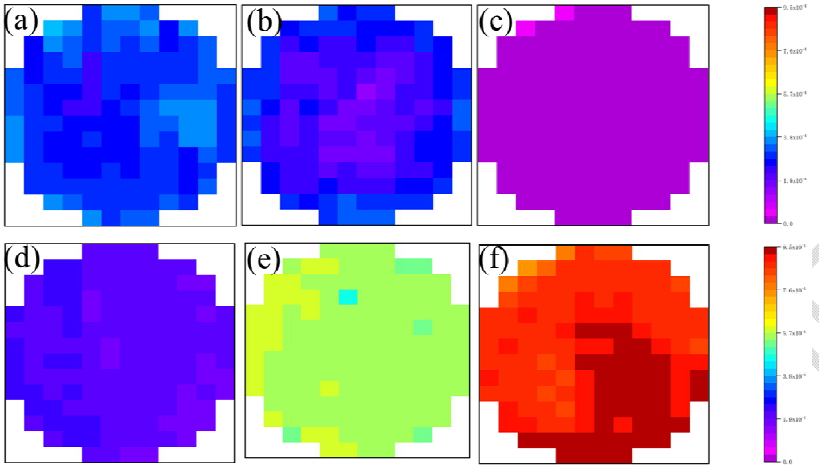

Fig. 6: HA concentration distribution on the membrane surface when the XG content is 25% and the filtration time is 5 min (a), 10 min (b), and 20 min (c).XG concentration distribution on the membrane surface when the XG content is 25% and the filtration time is 5 min (d), 10 min (e), and 20 min (f)

Fig. 6 showed the temporal and spatial distribution of pollutants on the membrane surface when the XG content was 25%.It could be seen from Fig. 6 that the pollutant distribution on the membrane surface was generally uniform.The concentration of HA on the membrane surface decreased with time, while the concentration of XG increased with time.When the filtration time was 5 minutes, the HA concentration on the membrane surface was slightly higher than that of XG. Therefore, the rapid decline of membrane flux in the first 5 minutes may be caused by the blockage of membrane pores by HA.When the filtration time reached 10 minutes, the membrane surface was obviously dominated by XG. When the filtration time reached 20 min, the XG concentration on the membrane surface was much higher than that of HA, which meant the influence of the pollution layer formed by XG on membrane fouling was significantly greater than that of HA.

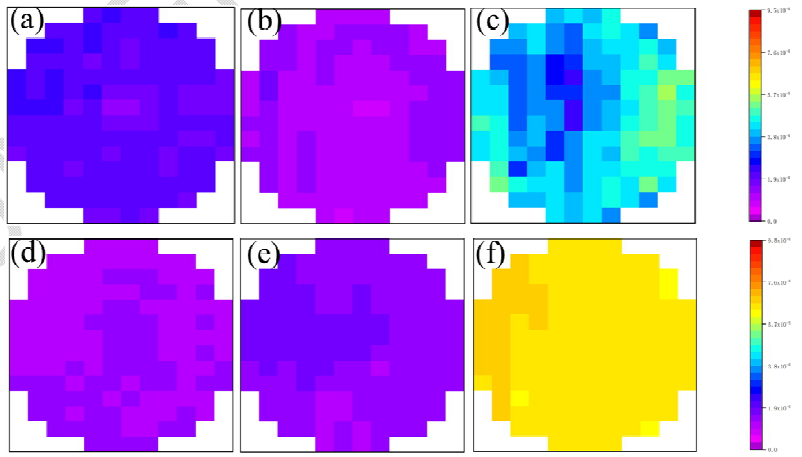

UNDER PEER REVIEW

Fig. 7 The HA concentration distribution on the membrane surface when the XG content is 60% and the filtration time is 5 min (a), 10 min (b), and 20 min (c).the XG concentration distribution on the membrane surface when the XG content is 60% and the filtration time is 5 min (d), 10 min (e), and 20 min (f),

Fig. 7 showed the dynamic changes of pollutants on the membrane surface when the XG content was 60%.The fouling degree of the membrane surface with 60% XG content was lighter than that with 25% XG content, which corresponded to the attenuation of membrane flux.In the first 10 minutes of the filtration process, the concentration ofHA or XG on the membrane surface changed little.When the filtration time reached 20 min, the concentration of pollutants on the membrane surface was higher than that before, and the concentration of XG was slightly higher than that of HA, indicating that XG had begun to form a pollution layer on the membrane surface.

3.4 Characterization of fouling morphology on the membrane surface

To understand the dynamic changes of membrane surface pollution more intuitively in the filtration process, the simulated water samples containing 25% XG with the most serious attenuation of membrane flux were selected. The membrane surface was characterized by SEM after 5 min, 10 min, and 20 min of modified membrane filtration.The morphology of the membrane surface under different filtration durations is shown in Fig. 8.When the filtration time was5min, the fouling layer on the membrane surface could be observed under1000times magnification. However, when the filtration time was10 min, there was no pore on the membrane surface, indicating that with the increase of filtration time, the fouling layer on the membrane surface would become denser.As shown in Fig. 8 (f), when the magnification was 20000 times and the filtration time was 20 min, the gel material could be obviously observed in the lower-left corner of SEM.This confirmed that XG could promote the formation of a gel layer on the membrane surface due to its gelation. Combined with the accumulation of HA on the membrane surface, the filtration resistance was increased, resulting in the decrease of membrane flux.

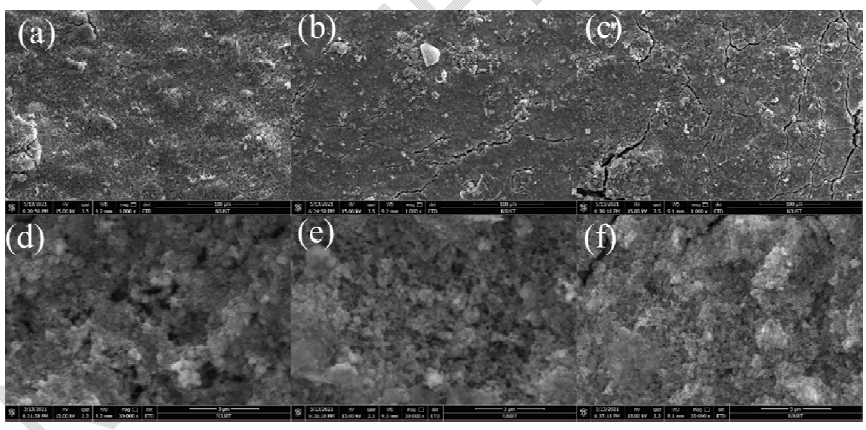

Fig. 8 The SEM image of the membrane surface after the nZVI/PVDF membrane filters 25%XG simulated wastewater for different filtration times. (A) 5 min, (b) 10 min, (c) 20 min magnification is 1000 times; (d) 5 min, (e) 10 min, (f) 20 min magnification is 20000 times.

This study showed that the mixture of humic acid and sodium alginate could affect nZVI@PVDF membrane fouling. A surprising finding was that the most serious pollution occurred when 75% HA and 25% XG are mixed, and the main pollutant on the membrane surface was XG after 1 h of the filtration cycle.From the fifth minute to twenty minutes, the concentration of XG was higher than HA. Similarly, the concentration of XG on the membrane surface was higher when

Comment [en10]: In the characterization section with SEM, how can the statement "This study showed that the mixture of humic acid and sodium alginate could affect nZVI@PVDF membrane fouling" be justified when the wastewater simulation procedure only referenced XG?

UNDER PEER REVIEW

pure XG and pure HA are filtered at the same concentration. These results showed that in the fouling process of the modified nZVI@PVDF membrane, the fouling layer formed mainly by XG on the surface, while the membrane pore blockage caused by HA had little effect on membrane fouling. XG has a high molecular weight and high viscosity at low concentration, which affected the filtration flux [29].In addition, XG has gel properties and bridges between molecules, forming a three-dimensional gel network on the membrane surface and accumulating on the membrane surface [30].Therefore, the macromolecular XG caused more serious pollution by blocking the membrane surface. In addition, due to the use of nZVI@PVDF modified membrane, the nZVI coated on the membrane surface will be beaded due to its magnetism, which will also promote the accumulation of XG on the membrane surface.The SEM images of the membrane surface in Fig. 8 confirmed that XG could promote the formation of a gel layer on the membrane surface due to its gelation. Combined with the accumulation of HA on the membrane surface, the filtration resistance was increased, resulting in the decrease of membrane flux and high TEP (84.65 mg Xeq/L). The concentration of pollutants on the membrane surface increased with time, and the main pollutants on the membrane surface changed due to the composition of water samples and filtration time.Overall, in the process of nZVI@PVDF membrane fouling in the mixed solution of XG and HA, the main contributor to the pollution was the pollution layer formed by XG on the surface of the membrane, while the pore blockage caused by HA had little effect on the membrane fouling.

More importantly, lighter membrane fouling occurred at 60 % XG concentration.The main pollutant on the membrane surface was HA when the filtration time was 1 h. In contrast, after 1 hour of pure HA filtration, the membrane flux decayed seriously, but the concentration of pollutants on the membrane surface was low. The membrane fouling was related to the TEP content in water samples which the higher the TEP content was accompanied the more serious the membrane fouling and the higher the membrane flux attenuation. However, the concentration of TEP was not proportional to the amount of XG when XG is 60%.This indicated that the interaction between HA and XG had an impact on the formation process of TEP in water samples, resulting in a new change in membrane surface pollution. This was because HA may enter the membrane pore and block the membrane pore.In our experiment, nZVI was chain-like on the membrane surface, so the average pore size of the nZVI layer was much larger than that of the HA molecule, resulting in many HA molecules not being intercepted by nZVI, and HA molecules could still reach the membrane surface, blocking the membrane pores in the filtration process.When 60% XG was mixed with HA, the XG concentration attached to the membrane surface was higher in the fifth to twentieth minutes.Subsequently, the gel network formed by XG captured HA, which made HA stay in the fouling layer on the membrane surface. HA was intercepted by the pollutants on the membrane surface, so the main pollutants on the membrane surface became HA. The mixed solution of HA and XG will basically aggravate the membrane fouling of the nZVI@PVDF membrane, but there may be a certain proportion range, which can reduce the membrane fouling, and even there is an optimal proportion, which can greatly reduce the membrane fouling.

4. CONCLUSION

In this study, we investigated the membrane fouling behavior of nZVI@PVDF membranes when exposed to varying concentrations of xanthan gum and humic acid, two key dissolved organic matter components. Our findings demonstrate that the interaction between XG and HA significantly impacts the formation of transparent exopolymer particles, which directly correlates with the degree of membrane fouling.The results indicate that XG plays a predominant role in membrane fouling, with the most severe fouling occurring at lower XG concentrations (25%) and the lightest fouling at 60% XG. This suggests that an optimal XG-to-HA ratio can mitigate fouling, offering valuable insights for enhancing the performance of modified membranes in water filtration processes. Furthermore, the use of advanced techniques such as infrared spectroscopy and multivariable curve resolution (MCR-ALS) enabled us to accurately characterize the fouling mechanisms and pollutant distribution on the membrane surface.These findings provide a foundation for developing more effective fouling control strategies in ultrafiltration systems, particularly those involving nanomaterial-modified membranes. Future research could explore the influence of other organic pollutants and further refine the optimal composition of dissolved organic matter to improve membrane longevity and filtration efficiency.

REFERENCES

[1] XIANG Y H, LIU F, XUE L X. Under seawater superoleophobic PVDF membrane inspired by polydopamine for efficient oil/seawater separation [J]. Journal of Membrane Science, 2015, 476: 321-329.

[2] TAWALBEH M, AL MOJJLY A, AL-OTHMAN A, HILAL N. Membrane separation as a pre-treatment process for oily saline water [J]. Desalination, 2018, 447: 182-202.

UNDER PEER REVIEW

[3] GURRERI L, TAMBURINI A, CIPOLLINA A, MICALE G. Electrodialysis Applications in Wastewater Treatment for Environmental Protection and Resources Recovery: A Systematic Review on Progress and Perspectives [J]. Membranes, 2020, 10(7): 146.

[4] YAO M, TIJING L, NAIDU G, et al. A review of membrane wettability for the treatment of saline water deploying membrane distillation [J]. Desalination, 2020, 479: 11472.

[5] YI X S, YU S L, SHI W X, et al. The influence of important factors on ultrafiltration of oil/water emulsion using PVDF membrane modified by nano-sized TiO2/Al2O3 [J]. Desalination, 2011, 281: 179-184.

[6] GAO W, LIANG H, MA J, et al. Membrane fouling control in ultrafiltration technology for drinking water production: A review [J]. Desalination, 2011, 272(1): 1-8.

[7] TOSCO T, PETRANGELI PAPINI M, CRUZ VIGGI C, SETHI R. Nanoscale zerovalent iron particles for groundwater remediation: a review [J]. Journal of Cleaner Production, 2014, 77: 10-21.

[8] TOSCO T, COïSSON M, XUE D, SETHI R. Zerovalent iron nanoparticles for groundwater remediation: Surface and magnetic properties, colloidal stability, and perspectives for field application [J]. Nanoparticles Featuring Electromagnetic Properties: From Science to Engineering, 2012: 201-223.

[9] QU X, ALVAREZ P J J, LI Q. Applications of nanotechnology in water and wastewater treatment [J]. Water Research, 2013, 47(12): 3931-3946.

[10] WANG X, YANG J, ZHU M, LI F. Characterization and regeneration of Pd/Fe nanoparticles immobilized in modified PVDF membrane [J]. Journal of the Taiwan Institute of Chemical Engineers, 2013, 44(3): 386-392.

[11] HERNáNDEZ S, PAPP J K, BHATTACHARYYA D. Iron-Based Redox Polymerization of Acrylic Acid for Direct Synthesis of Hydrogel/Membranes and Metal Nanoparticles for Water Treatment [J]. Industrial & Engineering Chemistry Research, 2014, 53(3): 1130-42.

[12] GUI M, ORMSBEE L E, BHATTACHARYYA D. Reactive Functionalized Membranes for Polychlorinated Biphenyl Degradation [J]. Industrial & Engineering Chemistry Research, 2013, 52(31): 10430-10440.

[13] LI N, CHEN H-D, LU Y-Z, et al. Nanoscale zero-valent iron-modified PVDF membrane prepared by a simple filter-press coating method can robustly remove 2-chlorophenol from wastewater [J]. Chemical Engineering Journal, 2021, 416: 127701.

[14] PEZESHK N, NARBAITZ R M. More fouling resistant modified PVDF ultrafiltration membranes for water treatment [J]. Desalination, 2012, 287: 247-54.

[15] LIU F, HASHIM N A, LIU Y T, et al. Progress in the production and modification of PVDF membranes [J]. Journal of Membrane Science, 2011, 375(1-2): 1-27.

[16] CHEN W, QIAN C, ZHOU K-G, YU H-Q. Molecular Spectroscopic Characterization of Membrane Fouling: A Critical Review [J]. Chem, 2018, 4(7): 1492-509.

[17] LOW S L, ONG S L, NG H Y. Characterization of membrane fouling in submerged ceramic membrane photobioreactors fed with effluent from membrane bioreactors [J]. Chemical Engineering Journal, 2016, 290: 91-102.

[18] ZHANG X, WANG Z, WU Z, et al. Formation of dynamic membrane in an anaerobic membrane bioreactor for municipal wastewater treatment [J]. Chemical Engineering Journal, 2010, 165(1): 175-183.

[19] NATARAJ S, SCHOMäCKER R, KRAUME M, et al. Analyses of polysaccharide fouling mechanisms during crossflow membrane filtration [J]. Journal of Membrane Science, 2008, 308(1): 152-161.

[20] XIAO F, XIAO P, ZHANG W J, WANG D S. Identification of key factors affecting the organic fouling on low-pressure ultrafiltration membranes [J]. Journal of Membrane Science, 2013, 447: 144-152.

UNDER PEER REVIEW

[21] BERMAN T, MIZRAHI R, DOSORETZ C G. Transparent exopolymer particles (TEP): A critical factor in aquatic biofilm initiation and fouling on filtration membranes [J]. Desalination, 2011, 276(1-3): 184-190.

[22] MENG S, WANG R, ZHANG K, et al. Transparent exopolymer particles (TEPs)-associated protobiofilm: A neglected contributor to biofouling during membrane filtration [J]. Frontiers of Environmental Science & Engineering, 2020, 15(4): 64.

[23] PASSOW U. Transparent exopolymer particles (TEP) in aquatic environments [J]. Progress in Oceanography, 2002, 55(3-4): 287-333.

[24] GAMAGE N P, CHELLAM S. Mechanisms of Physically Irreversible Fouling during Surface Water Microfiltration and Mitigation by Aluminum Electroflotation Pretreatment [J]. Environmental Science & Technology, 2014, 48(2): 1148-1157.

[25] ZHANG D, WANG P, SLIPCHENKO M N, CHENG J X. Fast vibrational imaging of single cells and tissues by stimulated Raman scattering microscopy [J]. Accounts of chemical research, 2014, 47(8): 2282-2290.

[26] FELTEN J, HALL H, JAUMOT J, et al. Vibrational spectroscopic image analysis of biological material using multivariate curve resolution–alternating least squares (MCR-ALS) [J]. Nature Protocols, 2015, 10(2): 217-40.

[27] CHEN W, LIU X-Y, HUANG B-C, et al. Probing Membrane Fouling via Infrared Attenuated Total Reflection Mapping Coupled with Multivariate Curve Resolution [J]. ChemPhysChem, 2016, 17(3): 358-363.

[28] MENG F, ZHANG S, OH Y, et al. Fouling in membrane bioreactors: An updated review [J]. Water Research, 2017, 114: 151-180.

[29] MENG S, LIU H, ZHAO Q, et al. Filtration Performances of Different Polysaccharides in Microfiltration Process [J]. Processes, 2019, 7(12): 897.

[30] MENG S J, LIU H J, ZHAO Q, et al. Filtration Performances of Different Polysaccharides in Microfiltration Process [J]. Processes, 2019, 7(12): 897.

UNDER PEER REVIEW